Received: April 20, 2023. Revised: June 25, 2023.

INASS

International Journal of
Intelligent Engineering & Systems

http://www.inass.org/

Brain Cancer Object Segmentation Using LPSIT Method and Back Propagation Network

B. Nisha[1]* M. Victor Jose[2]

[1]*Department of Computer Application, Noorul Islam Centre for Higher Education, Kumaracoil, K.K.Dist, Tamilnadu, India*
[2]*Department of Computer Science and Engineering*
Vel Tech Multi Tech Dr. Rangarajan Dr. Sakunthala Engineering College, Chennai, Tamilnadu, India.
* Corresponding author's Email: nisha_bernad@yahoo.co.in

Abstract: Brain cancer is the 10th leading cause of death for men and women. Magnetic resonance imaging (MRI) based Brain cancer segmentation is challenged by less accuracy and high time consumption, hence, an efficient cancer segmentation method is needed for the medical world. In this research, a novel brain cancer segmentation method on MRI is proposed which is entitled 'Brain cancer object Segmentation using LPSIT method and back propagation network (CS_LPSITBP)'. The own contribution of this paper is the 'Unsupervised segmentation of cancer object using Lanczos-3 interpolation based pyramidal structured iterative thresholding (LPSIT)'. The LPSIT method effectively segments the brain cancer region and delivers the key guidelines to generate the training sample to assist the back propagation neural (BPN) network. Processing of multi size images based pyramidal structure is the novel concept of this paper. A five-stage pyramidal based work is influenced in this paper. True positive rate (TPR) analysis reveals that the proposed CS_LPSITBP method improves the TPR by 1.92% compared to the next best method. Proposed method reaches the time consumption of 16.89 sec, while that of the next best method is only 23.88 sec. Experimental results in terms of FScore, Segmentation accuracy and MCR prove the efficiency of the proposed method compared with existing methods; hence, it can be used as a tool for medical practitioners.

Keywords: Brain cancer segmentation, Lanczos3 interpolation, Pyramidal structured iterative thresholding, Back propagation neural network, Medical image processing.

1. Introduction

Medical imaging analysis is important in identifying abnormalities in many human organs, such as brain, lung, and breast cancer. The brain is the most intricate organ in the human body. An improper mitotic mechanism affects the activity of morphological cells in the human brain. Malignant cells generated with different size and intensity morphological properties [1]. The potential use of medical images as biomarkers is to enhance the clinical outcomes and optimize the cancer therapy.

Strong magnetic and radio waves are used in magnetic resonance imaging (MRI). The diagnostic imaging algorithm is used to produce high-quality MRI scans of body organs that help in the diagnosis of malignancies and other illnesses like brain and spinal cord ailments [2]. Due to several circumstances, such as fatigue and an excessive number of MRI slices, the large-scale manual assessment method frequently results in misinterpretations.

The computer aided diagnosis (CAD) technique was created to identify brain cancers in their early stages without the use of a human. Based on MRI image, CAD systems can generate diagnostic reports and give the report to the radiologist. Many applications of fuzzy, neural networks, machine learning and deep learning in the field of medical imaging have significantly enhanced the CAD process. These algorithms improve the CAD system's accuracy in the detection of brain cancers [3].

The radiologist determines the manual segmentation, and there is significant intra- and inter variability. According on the degree of human involvement, there are three general categories for brain tumor segmentation: manual segmentation, semi-automated segmentation, and fully automatic segmentation. The automatic brain cancer detection system approach identifies the various brain disorders.

Ejaz et al. [4] described the hybrid segmentation algorithm for tumor region detection that integrates the component such as self organization feature map (SOM). The drawback of this technique is that it can be only applicable for MRI gray scale images. Dikici et al. [5] established the Brain Metastases (BM) framework for 3D MRI images. Demerit is the detection of only smaller brain Metastases. Saleeb et al. [6] bring out the technique for brain tumor detection using reconfigurable antenna array. This array-design only works for 2.4 GHz which is the defame of this work. Preethi et al. [7] delivered an image fusion algorithm for tumor detection and segmentation, using discrete wavelet transform, gray-level co-occurrence matrix and optimal deep neural network. The single classifier used in this paper reduces the accuracy which is the pitfall. Gajasinghe et al. [8] described a miniature system for tumor cell detection using micro fabricated EIS chip, printed circuit board, and data acquisition device. The weakness occurs from the similarity-based algorithm. Majib et al. [9] described a deep learning framework for brain tumor detection on MRI images. The downside is that this study only classifies brain tumors with 2D data. Salama et al. [10] established a Generative Model Framework for brain tumor detection and classification using deep models. The disadvantage is the slowest training in an offline stage. Shah et al. [11] bring out an algorithm for tumor detection using efficient-net model with fine-tuned layers. Drawback of this method is the high training time of deep convolutional neural network.

Dweik et al. [12] portrayed a filter for automatic segmentation of brain tumor in MRI images using geometrical active contours supported by the deep learning. Demerit is the inefficient contour initialization that significantly affects the accuracy. Ahuja et al. [13] delineated a super pixel technique for automatic brain tumor segmentation using T1 Weighted Magnetic Resonance Image datasets. The less powered volumetric analysis technique used in this paper limits the accuracy. Kronberg et al. [14] expressed an AI based brain tumor segmentation along with the segmentation of the necrotic nucleus, peritumoral edema and tumor enhancement. Demerit is the less accurate segmentation of Edema region due to its uncertainty level. Wang et al. [15] spelt out relax and focus approach for tumor segmentation using the limiting relaxation procedure that supports to internal boundary of the tumor. Demerit is the high time complexity. Akbar et al. [16] presented a single level UNET technique for brain tumor segmentation, which has the addition of attention in the skip connection. The essential calibration of UNET using hard parameters is a tough task which is the drawback.

Mathews et al. [32] described a brain tumor segmentation method using attention gate and compound loss. This method takes input from multi-model MRI. This method is not capable to handle the complex MRI images. Akbar et al. [33] reported a brain cancer segmentation method using Shallow dilated with attention Unet2,5D that works based on multi slices of MRI. The drawback is the limited dice segmentation performance.

Sharif et al. [25] described the binomial-thresholding, multi-features selection approach and Support Vector Machine (SVM) for cancer segmentation. The pitfall is that over-segmentation occurs when a tumor is developed in the border region. Chandra et al. [26] presented a mesh free model for tumor detection and segmentation using the selection of any spatial derivative order. It takes a considerable computational cost due to the usage of clustering method. Khan et al. [27] described the pyramidal based multi-scale method for brain tumor segmentation. The drawback is that it over segments or under segments the cancer region for severely affected images.

The existing algorithms are suffered by the challenges such as less segmentation accuracy, high false segmentation and high time complexity, hence, this paper proposed a new method for brain cancer segmentation entitled ‘Brain cancer object segmentation using LPSIT method and back propagation network (CS_LPSITBP)'. The proposed method is constructed by the following concepts:

- Lanczos-3 interpolation
- Processing of multi size images based pyramidal structure
- Iterative threshold approach
- Combined usage of unsupervised and supervised clustering
- Back propagation neural (BPN) network.

In this work, a multi size image-based network for brain cancer segmentation is proposed. Its intakes the grayscale brain MRI images and produces the

segmented version of brain cancer object in that MRI image.

Section 2 explains the working methodology of the proposed method. Section 3 explains the discussion and analysis on the proposed brain cancer segmentation method with various analytic measures. Section 4 describes the conclusion of the analysis part about the existing and proposed methods.

2. Proposed method

The proposed method is constructed by two core components, and they are:

1. Unsupervised segmentation of cancer object using Lanczos-3 interpolation based pyramidal structured iterative thresholding (LPSIT)
2. Back propagation neural (BPN) network-based cancer object segmentation.

In the proposed approach, the grayscale MRI is fed as input and it undergoes the skull removal process. The skull removed binary image and intensity image are used to segment the brain cancer object. The Fig.1 shows the overall diagram of the proposed CS_LPSITBP approach.

The LPSIT approach yields powerful unsupervised image segmentation. The iterative threshold computation by the decomposition of MRI image in the fashion of an essential Pyramidal structure is the new finding of the LPSIT approach. This approach partially determines the boundary of the cancer object using Lanczos3 interpolation to prepare the training feature-samples which can be treated as source of BPN training in the supervised style. Afterword, the trained-BPN determines the brain cancer region using the testing-BPN process, which reflects accurate cancer segmentation as the final output.

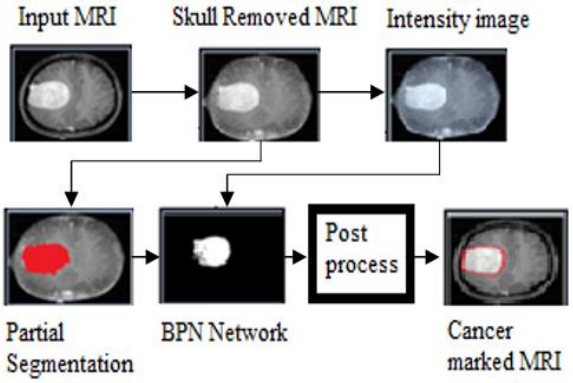

Figure. 1 Overall diagram for the proposed CS_LPSITBP approach

2.1 LPSIT approach based unsupervised cancer object segmentation

Unsupervised image segmentation spots the approximate cancer region automatically without the need of manual ground truth preparation. The traditional manual ground truth image-based training sample generation needs excess quality of cancer images; and also, it absorbs more time consumption for training. An enhanced unsupervised segmentation approach can trigger the supervised method to project high grade brain cancer segmentation. Therefore, this paper proposes a new unsupervised cancer region segmentation method entitled LPSIT. It is constituted by the concepts like Lanczos-3 interpolation and pyramidal structured iterative thresholding. This novel method acts a network to find the cancer region pixels.

The input MRI image is undergone the skull removal process using irrational mask which is explained in [28]. The output skull removed intensity image which consist only tissue image of brain MRI is given as input to the LPSIT approach. It formulates the approximately/partially separated brain cancer. The overall diagram of the LPSIT approach is described in Fig. 2. It can be sub-divided into six components like, 2^{n-4} stage, 2^{n-3} stage, 2^{n-2} stage, 2^{n-1} stage, 2^{n} stage, and Segmentation based on majority voting.

Herein, it can be considered as the process of pyramidal shape that can be accomplished through the smallest dimensional image 2^{n-4}, and the sequentially bigger levels such as 2^{n-3}, 2^{n-2}, 2^{n-1}, and 2^{n}. The Fig. 3 exposes the connections between the layers of the proposed network which is influenced by the images of five levels of progressively increased dimensions. The outputs of intermediate binary segmentation are connected to next level. Intervals are reorganized in every iteration. The segmented cancer object is segregated based on voting oriented approach.

Procedure of 2^{n-4} stage

Down sampling process reduces the image dimension into a specific size. Up sampling increases resolution of an image. This component absorbs the 'skull removed tissue image' as input which can be referred I_{TS}. The size of it is 256×256 and it consists only the tissue region, where the background is filled by zeros. Lanczos-3 interpolation performs better than the other interpolation approaches such as nearest neighbor interpolation, Tri-linear interpolation and Tricubic interpolation [17]. It works based on the dynamic Lanczos kernel. It estimates the info in the directions of horizontal and vertical, and finally the depth direction is proceeded using the 3D

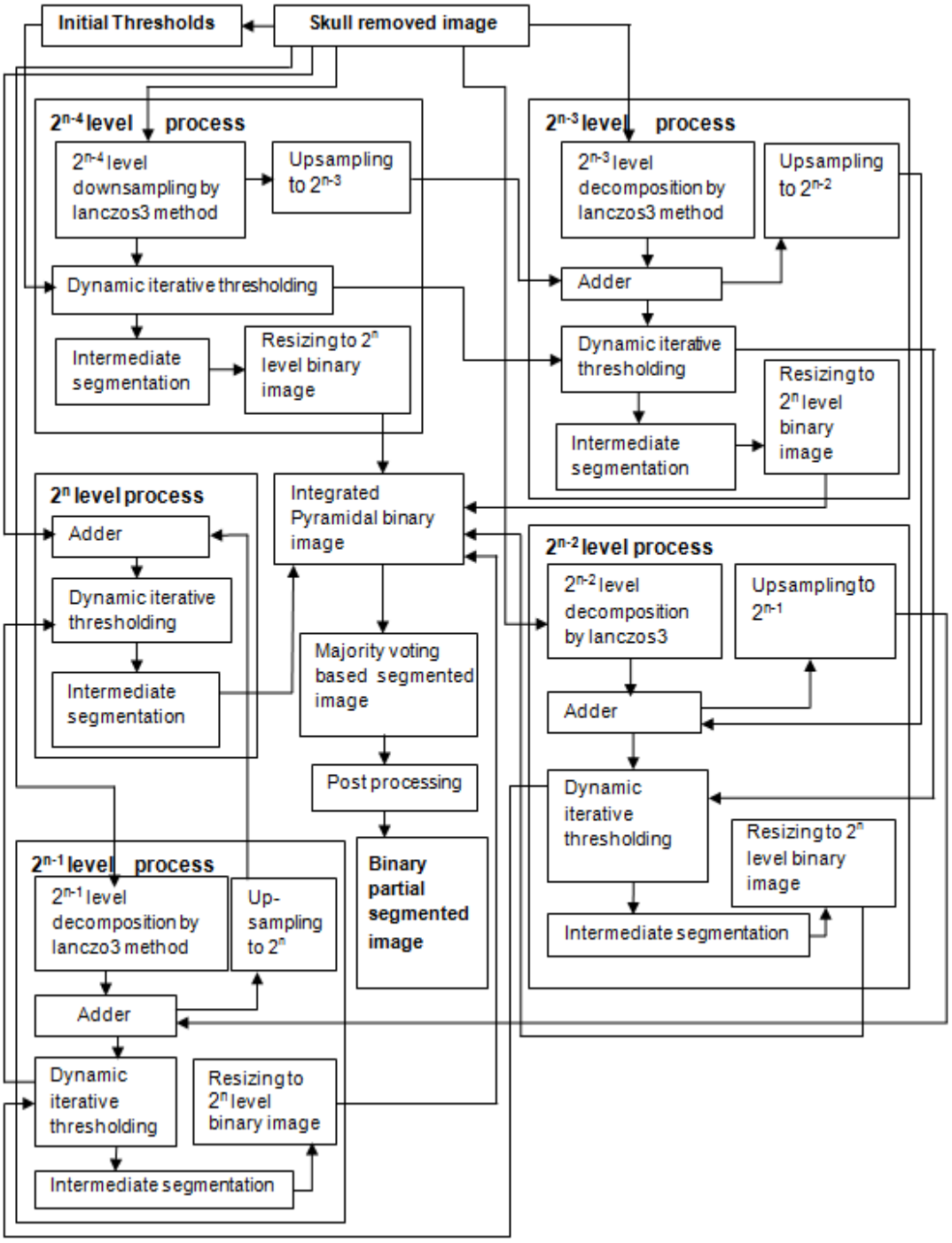

Figure. 2 Block diagram of the proposed LPSIT approach

interpolation to get the improved edge sharpness and reduced artifacts [18]. Hence, this paper uses the Lanczos-3 interpolation to get multi size images by resizing process. Consider the size of the tissue image I_{TS} is $2^n \times 2^n$. and it is shown in Fig. 4 (a). Based on Fig. 2, the I_{TS}image is reduced to $2^{n-4} \times 2^{n-4}$size via Lanczos-3 interpolation and it is shown in Fig. 4 (b). The Eq. (1) demonstrates this process.

$$I_{DS16\times16} = FuncLanczos3(I_{TS}, 2^{n-4} \times 2^{n-4}) \quad (1)$$

Herein, the term $FuncLanczos3$ represents the function to compute Lanczos-3 interpolation and $I_{DS16\times16}$ represents the downsampled version image related to $2^{n-4} \times 2^{n-4}$ size.

In Eq. (1), the $FuncLanczos3$ reduces the I_{TS} image to the size of 16×16 which is the simple outline of $2^{n-4} \times 2^{n-4}$ size against the input image size of 256×256.

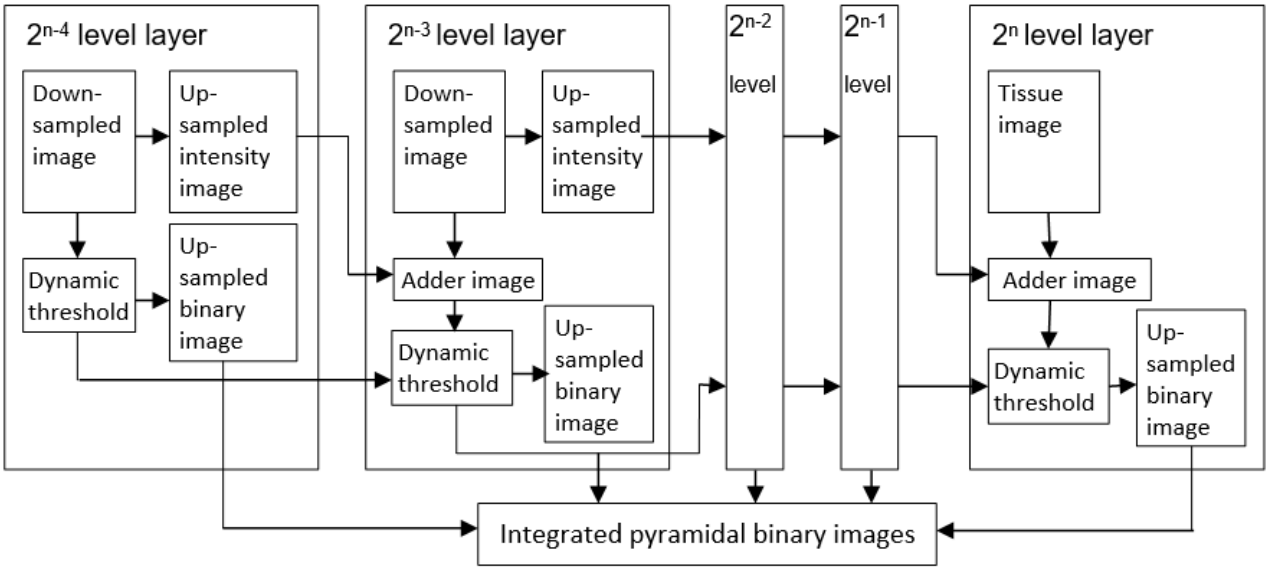

Figure. 3 Diagram to expose the connections between the pyramidal network

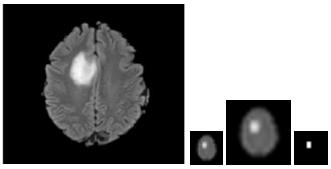

(a) (b) (c) (d)

Figure. 4 Demonstration of 2^{n-4} stage process

The Otsu's threshold approach [19] calculates the threshold in the initial iteration process using the maximum value detection process, which is revealed by Eq. (2), Eq. (3) and Eq. (4).

$$T_0 = FuncOtsu(I_{DS16\times16}) \tag{2}$$

$$T_1 = FuncMax(I_{DS16\times16}) \times th \tag{3}$$

$$T = FuncMax(T_0, T_1) \tag{4}$$

Herein, the term T_0 refers the threshold value by Otsu algorithm, T_1 refers the threshold value corresponding to maximum, T refers the threshold of initial occurrence, th refers the experimental oriented threshold which can be 0.8, $FuncOtsu$ refers the function to calculate the Otsu based threshold, and F$uncMax$ refers the function to find the maximum value of intensity. A global oriented threshold is calculated based on Otsu approach. Afterwards, Eq. (3) calculates the T_1 via the hard-threshold th. The term th is found in the manner of multiple experimental trials. Initial threshold is chosen with the help of T_0 and T_1 by the maximum parameter detection.

The separation between foreground and background data is progressed by initial threshold to generate the binary segmented image I_{BS}, which can be illustrated by Eq. (5).

$$I_{BS}^{i,j} = \begin{cases} 1, & if\ I_{DS16\times16}^{i,j} > T \\ 0, & otherwise \end{cases}, i \in [0, 2^{n-4}-1], \quad j \in [0, 2^{n-4}-1] \tag{5}$$

Soft threshold TH_0 related to 2^{n-4} stage is computed via Eq. (6) using two parameters such as mean of foreground-intensity M_F and mean of background- intensity M_B. The M_F and M_B are determined from the binary image I_{BS}.

$$TH_0 = \frac{(M_F + M_B)}{2} \tag{6}$$

Dynamic threshold TH_0 generates the intermediate segmented binary image $I_{B16\times16}$ via Eq. (7).

$$I_{B16\times16}^{i,j} = \begin{cases} 1, & if\ I_{DS16\times16}^{i,j} > TH_0 \\ 0, & otherwise \end{cases}, i \in [0, 2^{n-4}-1], \ j \in [0, 2^{n-4}-1] \tag{7}$$

The 'imresize' function of MATLAB makes the upsampled segmented binary image I_{UBS0} in the size of $2^n \times 2^n$, and the output is shown in Fig. 4 (d). Upsampled intensity image $I_{UI32\times32}$ is generated via Lanczos-3 algorithm using the $I_{DS16\times16}$ image, and it is shown in Fig. 4 (c).

Procedure of 2^{n-3} stage

Lanczos3 interpolation is applied on I_{TS} to get the downsampled image $I_{DS32\times32}$ in the size of $2^{n-3} \times 2^{n-3}$ via Eq. (8).

$$I_{DS32\times32} = FuncLanczos3(I_{TS}, 2^{n-3} \times 2^{n-3}) \quad (8)$$

Adding process is done on downsampled version image $I_{DS32\times32}$ and upsampled version intensity image $I_{UI32\times32}$, based on Eq. (9) and the Adder image is quoted as $I_{ADD32\times32}$.

$$I_{ADD32\times32} = \frac{(I_{DS32\times32}+I_{UI32\times32})}{2} \quad (9)$$

Updated dynamic threshold corresponding to 2^{n-3} stage process is calculated using the dynamic threshold TH_0. Binarization is performed to separate the foreground and background data in Adder image $I_{ADD32\times32}$ using Eq. (10).

$$I_{BS}^{i,j} = \begin{cases} 1, & if\ I_{ADD32\times32}^{i,j} > TH_0 \\ 0, & otherwise \end{cases}, i \in [0, 2^{n-3}-1], \quad j \in [0, 2^{n-3}-1] \quad (10)$$

The foreground mean intensity M_F and background mean intensity M_B are computed using the values of $1s$ and $0s$. The updated dynamic threshold corresponding to 2^{n-3} stage which is noted by TH_1, is calculated using Equ.6. The intermediate segmented binary image $I_{B32\times32}$ is formed based on the dynamic threshold TH_1 using Eq. (11).

$$I_{B32\times32}^{i,j} = \begin{cases} 1, & if\ I_{ADD32\times32}^{i,j} > TH_1 \\ 0, & otherwise \end{cases}, i \in [0, 2^{n-3}-1],\ j \in [0, 2^{n-3}-1] \quad (11)$$

Upsampling process is performed to reach the dimension of $2^n \times 2^n$ to get the upsampled binary image I_{UBS1}. The Adder intensity image $I_{ADD32\times32}$ is upsampled using Lanczos3 interpolation to reach the upsampled intensity image $I_{UI64\times64}$ that have the dimension of $2^{n-2} \times 2^{n-2}$.

Procedure of 2^{n-2} stage

The downsampled image $I_{DS64\times64}$ is obtained from I_{TS} by utilizing the Lanczos3 algorithm in the size of $2^{n-2} \times 2^{n-2}$.

The images such as $I_{DS64\times64}$ and $I_{UI64\times64}$ are used to get the Adder image $I_{ADD64\times64}$. Updated dynamic threshold is computed using TH_1. The $I_{ADD64\times64}$ image undergone the binarization using TH_1 to separate the foreground and background. Updated dynamic threshold TH_2 is found by Eq. (6) from M_F and M_B. The Eq. (7) uses the TH_2 to form the intermediate segmented binary image $I_{B64\times64}$. The image $I_{B64\times64}$ formulates the up sampled binary image I_{UBS2} in the dimension of $2^n \times 2^n$. Lanczos3 algorithm makes an up sampling on $I_{ADD64\times64}$ to the size of $2^{n-1} \times 2^{n-1}$ to construct the upsampled intensity image $I_{UI128\times128}$.

Procedure of 2^{n-1} stage

Lanczos3 algorithm downsamples the I_{TS} image to the dimension of $2^{n-1} \times 2^{n-1}$ and it is quoted as $I_{DS128\times128}$. Adder version image $I_{ADD128\times128}$ is generated via the images such as $I_{DS128\times128}$ and $I_{UI128\times128}$. The threshold quoted by TH_2 helps to calculate the updated dynamic threshold TH_3 which is related to 2^{n-1} stage by using the image of $I_{ADD128\times128}$. Intermediate binary segmented image $I_{B128\times128}^{i,j}$ is constructed using binarization process. The upsampled binary image I_{UBS3} is set with the size of $2^n \times 2^n$.The $I_{ADD128\times128}$ image is used as the source to derive the upsampled intensity image $I_{UI256\times256}$ in the size of $2^n \times 2^n$.

Procedure of 2^n stage

Adder image $I_{ADD256\times256}$ is generated using Tissue image I_{TS} and upsampled intensity image $I_{UI256\times256}$) using Eq. (12).

$$I_{ADD256\times256} = \frac{(I_{TS}+I_{UI256\times256})}{2} \quad (12)$$

Dynamic threshold TH_3 is used to compute the updated dynamic threshold TH_4 corresponding to 2^n stage from $I_{ADD256\times256}$ image. The binary segmented image I_{BS4} is generated using the threshold TH_4 in the dimension of $2^n \times 2^n$.

Segmentation based on majority voting

A majority-based voting process is employed on the aforementioned binary images using Eq. (13).

$$I_{ADDER} = I_{UBS0} + I_{UBS1} + I_{UBS2} + I_{UBS3} + I_{BS4} \quad (13)$$

$$I_{BCS}^{i,j} = \begin{cases} 1, if\ I_{ADDER}^{i,j} \geq 2, i \in [0, 2^n-1], j \in [0, 2^n-1] \\ 0, \ otherwise \end{cases} \quad (14)$$

Herein, the term I_{ADDER} refers the Adder image of five binary segmented images, and I_{BCS} refers the Binary cancer segmented image. In Eq. (14), the pixels which belongs to the majority state are assigned by 1 and others are assigned by 0. Herein, if the pixel value is more than or equal to 2, then the majority state is confirmed. The threshold 2 is fixed based on multiple trials of execution of this majority voting-based system. I_{ADDER} image contains the data range of 0 to 5. The resultant binary segmented image $I_{BCS}^{i,j}$ is undergone the post process which eliminates

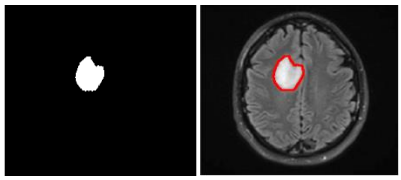

(a) (b)

Figure. 6 BPN based cancer region segmentation: (a) binary segmented image and (b) cancer marked image

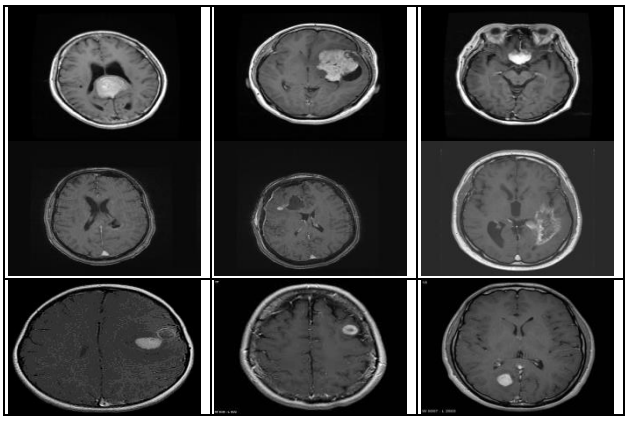

Figure 7. Demonstration of sample database images

small size noisy objects.

The output of adder image I_{ADDER} contains a blurring in edges. The data range of this image is 0 to 5. The $I_{BCS}^{i,j}$ image is the final output of the proposed LPSIT approach.

2.2 Back propagation neural (BPN) network based cancer object segmentation

Back propagation neural (BPN) network is a type of supervised machine learning that determines the gradient of the loss function, which measures how a forecast differs from actual outcomes. There are 3 layers in the BPN architecture viz. input layer, hidden layers and output layer [20]. The output of LPSIT method act as a guideline to extract the features for training feature samples which can be fed to BPN network. Skull removed intensity image is undergone the test samples extraction process.

The 'Tissue & background region' and 'Cancer region' oriented individual features are extracted in the form of features such as Statistical, texture and intensity. Statistical features [21, 22, 23] such as arithmetic mean, variance, standard deviation and regression, Textural features [24, 22] such as correlation, energy, entropy and contrast, and Intensity feature from 3×3 window are extracted to fix the final 17 features.

The BPN network is created by setting the number of input layer as 17 with double hidden layers formed by 10 nodes. A single output layer is fixed with a single node. The maximum number of iterations is calibrated to 250, learning rate is fixed to 0.93 along with the Error-Goal of 0.00001. Thousand tissue-oriented features are extracted from the 'skull removed intensity' image using the window size of 3×3 by utilizing the 'skull removed binary' image as a guideline. Features of cancer region is extracted from the 'skull removed intensity' image using the window size of 3×3 by utilizing the binary segmented image I_{BCS} as a guideline. Target value is set to 0 for tissue area and 1 for cancer area. BPN network is trained using the above settings.

Test-features are derived from Skull removed intensity image to test the trained network. Testing process is progressed only in the tissue area noted by the skull removed binary version image. Cancer pixel are identified by validating the pixel data nearer to 1 and other pixels are identified as non-cancer pixels. Noises like small objects are eliminated using the post-process and the final output is noted as I_{FBC}, which is set in Fig. 6 (a). Cancer region is marked by red color in the final cancer segmented image and shown in Fig. 6 (b). Thus, the proposed CS_LPSITBP method segments the cancer region.

3. Discussion and analysis

Proposed CS_LPSITBP approach is analyzed using the three databases such as Kaggle brain tumor image dataset (KBTD_DS) [29], Brain images of tumors for evaluation dataset (BITE_DS) [30], and Figshare brain tumor dataset (FBTD_DS) [31]. Fig. 7 shows the sample images from the three databases. The first row in Fig. 7 demonstrates the FBTD_DS database samples, second row shows the BITE_DS database samples and third row depicts the KBTD_DS database samples.

The three existing approaches listed below are used for analysis purpose.

- Brain Cancer segmentation using improved binomial-thresholding and multi-features selection (BCS_IBM) [25]
- Brain cancer segmentation using mesh-free super-diffusive model (BCS_MSM) [26]
- Brain cancer segmentation using pyramid based multi-scale encoder-decoder network (BCS_PMN) [27].

True positive rate (TPR) is also known as sensitivity. Higher TPR shows the better-quality brain cancer segmentation. TPR is computed in the unit of percentage (%).

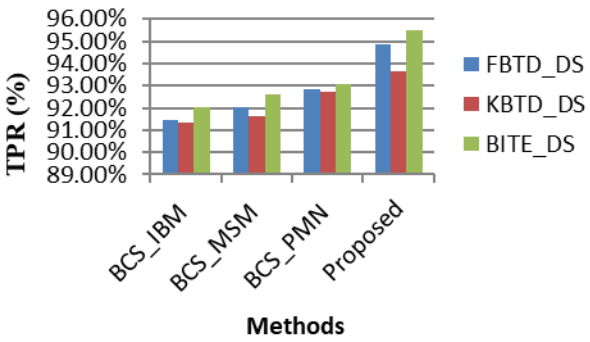

Figure 8.True positive rate (TPR) analysis chart for cancer segmentation

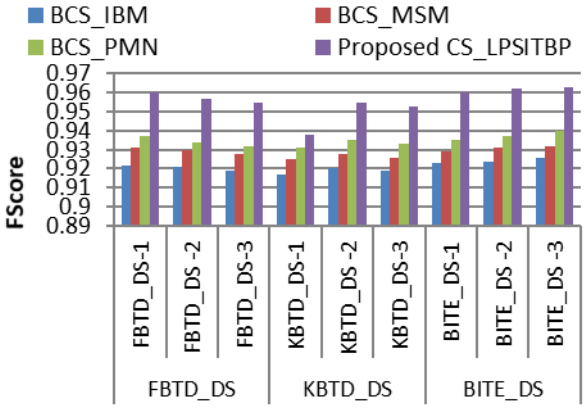

Figure. 9 FScore analysis for cancer segmentation

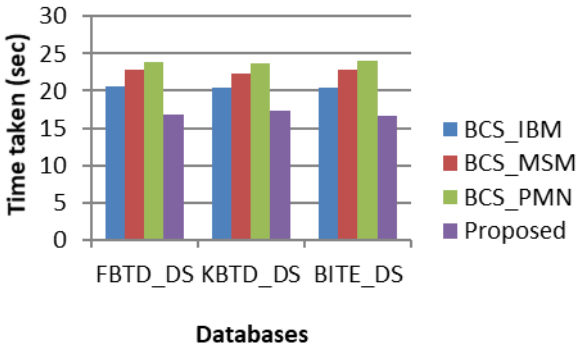

Figure 10. Time-taken analysis for cancer segmentation

Fig. 8 demonstrates the PR analysis and the proposed approach has the maximum TPR 95.51% related to BITE_DS database. The proposed method has the high average TPR value than the existing versions.

FScore measure is influenced by the two parameters such as Precision and Recall. Fig. 9 shows the FScore assessment for segmenting cancer objects. highest FScore 0.9632 is achieved by the proposed approach corresponding to the BITE_DS-3 image. Hence, BITE_DS database is the best supportive database for brain cancer segmentation.

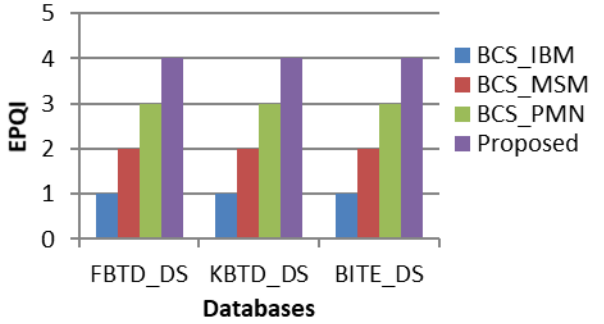

Figure. 11 EPQI analysis chart

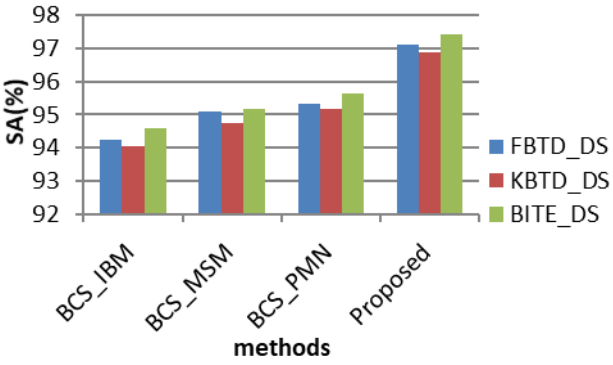

Figure. 12 Analysis on segmentation accuracy for segmenting cancer objects

Table 1. Average misclassification ratio analysis for cancer segmentation

Database	MCR of cancer segmentation (%)			
	BCS_ IBM	BCS_ MSM	BCS_ PMN	Proposed
KBTD_DS	5.96	5.23	4.80	**3.10**
BITE_DS	5.38	4.81	4.37	**2.56**
FBTD_DS	5.75	4.91	4.66	**2.89**

Time taken (TT) analysis is shown in Fig. 10. The CS_LPSITBP algorithm consumes less time when comparing the previous algorithms, i.e., the least time of 16.65 seconds is consumed related to BITE_DS dataset.

Seven human observers involved to inspect the segmentation quality of considered algorithms via eye perception. This assessment is called eye perception based quality index (EPQI).

Fig. 11 displays the EPQI analysis. Proposed CS_LPSITBP algorithm achieves higher index value of 4 which denotes better output quality of the CS_LPSITBP algorithm.

Segmentation accuracy (SA) measure is progressed to evaluate the considered algorithms.

Fig. 12 exhibits the segmentation accuracy assessment and the CS_LPSITBP algorithm obtains the higher segmentation accuracy for cancer separation.

MCR refers the ratio of estimations which are

Table 2. Average SA and TT assessment for brain cancer separation

Methods	Avg. SA (%)	Avg. TT (sec)
BCS_IBM	94.30	20.45
BCS_MSM	95.01	22.69
BCS_PMN	95.38	23.88
Proposed	**97.14**	**16.89**

erroneous, and the parameters such as true positive (TP), true negative (TN), false positive (FP) and false negative (FN) involved to this compute MCR via Eq. (15).

$$MCR = \frac{FP + FN}{TP + TN + FP + FN} \quad (15)$$

Less MCR defines the better result in segmentation of brain cancer. Hundred test images involved to compute the average MCR from every dataset, and the results are tabulated in Table 1. Proposed CS_LPSITBP algorithm acquires the least MCR than the previous algorithms. BITE_DS database is the best supportive dataset because it yields the lowest MCR value with respect to the CS_LPSITBP algorithms. Overall average MCR values are 5.70, 4.989, 4.614 and 2.856 against the four algorithms such as BCS_IBM, BCS_MSM, BCS_PMN and the proposed CS_LPSITBP respectively.

Table 2 shows the average SA and average time measure analysis for segmenting the brain cancer. The average SA is computed by averaging the SA values related to the three databases. Proposed approach produces the higher average SA (i.e., 97.144%) when compared to existing versions. Lower average TT (i.e., 16.897 sec) is yielded by the CS_LPSITBP algorithm which is the proof for the fastest execution on case of brain cancer segmentation.

The proposed work solves the issues of the existing methods, such as high time consumption and less accuracy. Moreover, it is a reliable work in brain tumor segmentation. It solves the issue of high hardware conversion cost due to its less complex architecture.

4. Conclusions

This paper progresses a new segmentation algorithm to segment the brain cancer from MRI images, which is entitled CS_LPSITBP. The main contribution of this work is the LPSIT algorithm which can segment cancer objects in unsupervised manner. Afterwards, the supervised model component constructed by BPN segments the cancer object efficiently. The LPSIT method and BPN empowers the proposed CS_LPSITBP method to produce top grade performance quality along with scaling issue, accuracy issue and time complexity. Standard analytic metrics proves the effectiveness of the proposed method in terms of segmentation accuracy, time taken, etc. The average segmentation accuracy and time taken value for the proposed CS_LPSITBP method are 97.14% and 16.89sec respectively. When compared to the existing methods, the proposed CS_LPSITBP method is declared as the best method for brain cancer detection and segmentation.

Appendix:

I_{TS} - skull removed tissue image
$I_{DS16\times16}$, $I_{DS32\times32}$, $I_{DS64\times64}$, $I_{DS128\times128}$ - Down-sampled version images
T_0 - Threshold value by Otsu algorithm
T_1 - Threshold value corresponding to maximum
T - Threshold of initial occurrence
I_{BS} - Binary segmented image
TH_0 , TH_1 , TH_2 , TH_3 , TH_4 - Dynamic thresholds
M_F - Mean of foreground-intensity
M_B - Mean of background- intensity
$I_{B16\times16}$, $I_{B32\times32}$, $I_{B64\times64}$, $I_{B128\times128}$ - Intermediate segmented binary images
$I_{UI32\times32}$, $I_{UI64\times64}$, $I_{UI128\times128}$, $I_{UI256\times256}$ - Upsampled version intensity images
$I_{ADD32\times32}$, $I_{ADD64\times64}$, $I_{ADD128\times128}$, $I_{ADD256\times256}$ - Adder images
I_{UBS1} , I_{UBS2} , I_{UBS3} , - Upsampled binary images
I_{BS4} - Binary segmented image for $2^n \times 2^n$
I_{ADDER} - Adder image of 5 binary segmented images
I_{BCS} - Binary cancer segmented image
I_{FBC} - Final binary cancer segmented image

Conflicts of interest

The authors declare that they have no conflict of interest.

Author contributions

The authors confirm contribution to the paper as follows: Study conception and design: B. Nisha and M. Victor Jose; Data collection: B. Nisha; Analysis and interpretation of results: M. Victor Jose; Draft manuscript preparation: B. Nisha and M. Victor Jose. All authors reviewed the results and approved the final version of the manuscript.

Acknowledgments

The authors would like to thank the reviewers for all of their careful, constructive and insightful comments in relation to this work.

References

[1] T. Saba, "Recent advancement in cancer detection using machine learning: Systematic survey of decades, comparisons and challenges", *Elsevier, Journal of Infection and Public Health*, Vol. 13, No. 9, pp. 1274-1289, 2020.

[2] R. Hajjo, D. A. Sabbah, S. K. Bardaweel, and A. Tropsha, "Identification of tumor-specific MRI biomarkers using machine learning (ML)", *Diagnostics*, Vol. 11, No. 5, pp. 1-27, 2021.

[3] M. S. I. Khan, A. Rahman, T. Debnath, M. R. Karim, M. K. Nasir, S. S. Band, A. Mosavi, and I. Dehzangi, "Accurate brain tumor detection using deep convolutional neural network", *Elsevier, Comput. Struct. Biotechnol. J.*, Vol. 20, pp. 4733-4745, 2022.

[4] K. Ejaz, M. S. M. Rahim, U. I. Bajwa, H. Chaudhry, A. Rehman, and F. Ejaz, "Hybrid segmentation method with confidence region detection for tumor identification", *IEEE Access*, Vol. 9, pp. 35256-35278, 2020.

[5] E. Dikici, J. L. Ryu, M. Demirer, M. Bigelow, R. D. White, W. Slone, B. S. Erdal, and L. M. Prevedello, "Automated brain metastases detection framework for T1-weighted contrast-enhanced 3D MRI", *IEEE J. Biomed. Health. Inf.*, Vol. 24, No. 10, pp. 2883-2893, 2020.

[6] D. A. Saleeb, R. M. Helmy, N. F. Areed, M. Marey, W. M. Abdulkawi and A. S. Elkorany, "A technique for the early detection of brain cancer using circularly polarized reconfigurable antenna array", *IEEE Access*, Vol. 9, pp. 133786-133794, 2021.

[7] S. Preethi and P. Aishwarya, "An efficient wavelet-based image fusion for brain tumor detection and segmentation over PET and MRI image", *Multimedia Tools Appl.*, Vol. 80, No. 10, pp. 14789-14806, 2021.

[8] R. W. Gajasinghe, B. Bougenot, M. A. Jones, T. A. Ince, and O. Tigli, "Miniaturized system for tumor cell detection and differentiation", *IEEE Sens. J.*, Vol. 21, No. 18, pp. 19697-19704, 2021.

[9] M. S. Majib, M. M. Rahman, T. S. Sazzad, N. I. Khan, and S. K. Dey, "Vgg-scnet: A vgg net-based deep learning framework for brain tumor detection on MRI images", *IEEE Access*, Vol. 9, pp. 116942-116952, 2021.

[10] W. M. Salama and A. Shokry, "A novel framework for brain tumor detection based on convolutional variational generative models", *Multimedia Tools Appl.*, Vol. 81, No. 12, pp. 16441-16454, 2022.

[11] H. A. Shah, F. Saeed, S. Yun, J. H. Park, A. Paul, and J. M. Kang, "A robust approach for brain tumor detection in magnetic resonance images using fine-tuned efficient net", *IEEE Access*, Vol. 10, pp. 65426-65438, 2022.

[12] M. Dweik and R. Ferretti, "Integrating anisotropic filtering, level set methods and convolutional neural networks for fully automatic segmentation of brain tumors in magnetic resonance imaging", *Neurosci. Inf.*, Vol. 2, No. 3, pp. 1-12, 2022.

[13] S. Ahuja, B. K. Panigrahi, and T. K. Gandhi, "Enhanced performance of dark-nets for brain tumor classification and segmentation using colormap-based superpixel techniques", *Mach. Learn. Appl.*, Vol. 7, pp. 1-13, 2022.

[14] R. M. Kronberg, D. Meskelevicius, M. Sabel, M. Kollmann, C. Rubbert, and I. Fischer, "Optimal acquisition sequence for AI-assisted brain tumor segmentation under the constraint of largest information gain per additional MRI sequence", *Neurosci. Inf.*, Vol. 2, Issue 4, pp. 1-10, 2022.

[15] P. Wang and A. C. Chung, "Relax and focus on brain tumor segmentation", *Med. Image Anal.*, Vol. 75, pp. 1-14, 2022.

[16] A. S. Akbar, C. Fatichah, and N. Suciati, "Single level UNet 3D with multipath residual attention block for brain tumor segmentation", *Journal of King Saud University-Computer and Information Sciences*, Vol. 34, pp. 3247-3258, 2022.

[17] T. Moraes, P. Amorim, J. Silva, and H. Pedrini, "3D Lanczos interpolation for medical volumes", In: *Proc. of 15th International Symposium on Computer Methods in Biomechanics and Biomedical Engineering*, pp. 1-10, 2018.

[18] B. N. Madhukar and R. Narendra, "Lanczos resampling for the digital processing of remotely sensed images", In: *Proc. of International Conference on VLSI, Communication, Advanced Devices, Signals & Systems and Networking* (VCASAN-2013), pp. 403-411, 2013.

[19] N. Otsu, "A threshold selection method from gray-level histograms", *IEEE Trans. Syst. Man Cybern.: Syst.*, Vol. 9, No. 1, pp. 62-66, 1979.

[20] I. Sanubary, "Brain tumor detection using back propagation neural networks", *Indonesian Journal of Physics and Nuclear Applications*, Vol. 3, No. 3, pp. 83-88, 2018.

[21] M. Ilamathi and P. Sumathy, "Shape based image classification using geometric properties", *J. Eng. Tech. Manage.*, Vol. 6, Issue 9, pp. 630-636, 2019.

[22] G. Malu, "A study on different feature extraction techniques for lesion identification in MRI breast images", *Indian J. Comput. Sci. Eng.*, Vol. 7, No. 5, pp. 189-202, 2016.

[23] A. M. H. Navarro, H. J. Hernandez, H. P. Barreto, F. M. Guerrero, and I. R. T. Villalobos, "A new measure of circularity based on distribution of the radius", *Computacion y Sistemas*, Vol. 17, No. 4, pp. 515-526, 2013.

[24] A. Chauguleand S. N. Mali, "Evaluation of texture and shape features for classification of four paddy varieties", *Journal of Engineering*, Vol. 2014, Article ID: 617263, 2014.

[25] M. Sharif, U. Tanvir, E. U. Munir, M. A. Khan, and M. Yasmin, "Brain tumor segmentation and classification by improved binomial thresholding and multi-features selection", *Springer, J. Ambient Intell. Hum. Comput.*, DOI: 10.1007/s12652-018-1075-x, pp. 1-20, 2018.

[26] S. K. Chandra and M. K. Bajpai, "Brain tumor detection and segmentation using mesh-free super-diffusive model", *Springer, Multimedia Tools Appl*, Vol. 79, No. 3, pp. 2653-2670, 2020.

[27] A. Khan, H. Kim, and L. Chua, "PMED-net: Pyramid based multi-scale encoder-decoder network for medical image segmentation", *IEEE Access*, Vol. 9, pp. 55988-55998, 2021.

[28] S. Moldovanu, L. Moraru, and A. Biswas "Robust skull-stripping segmentation based on irrational mask for magnetic resonance brain images", *Journal of Digit Imaging*, Vol. 28, pp. 738-747, 2015.

[29] KBTD-DS, 2021, Available from: <https://www.kaggle.com/navoneel/brain-mri-images-for-brain-tumor-detection>, accessed on [06 March 2021].

[30] BITE-DS, 2021, Available from: <nist-mni-mcgill.ca/?page=id=672>, accessed on [06 March 2021].

[31] FBTD-DS, 2021, Available from: <https://figshare.com/articles/dataset/ brain-tumor-dataset/ 1512427>, accessed on [06 March 2021].

[32] C. Mathews and A. Mohamed, "Nested U-Net with enhanced attention gate and compound loss for semantic segmentation of brain tumor from multimodal MRI", *International Journal of Intelligent Engineering and Systems*, Vol. 15, No. 4, pp. 248-256, 2022, doi: 10.22266/ijies2022.0831.23.

[33] A. S. Akbar, C. Fatichah, and N. Suciati, "SDA-UNET2.5D: Shallow dilated with attention Unet2.5D for brain tumor segmentation", *International Journal of Intelligent Engineering and Systems*, Vol. 15, No. 2, pp. 135-149, 2022, doi: 10.22266/ijies2022.0430.14.